World Journal of Advanced Research and Reviews
eISSN: 2581-9615 CODEN (USA): WJARAI
Cross Ref DOI: 10.30574/wjarr
Journal homepage: https://wjarr.com/

(RESEARCH ARTICLE)

Check for updates

Computational study of phytochemical derived bioactive compounds of *Vernonia amygdalina* as a potential inhibitor of Topoisomerase IV in pneumonia

Ayobami Fidelix [1,*], Tomilola Akingbade [2], Jatin Jangra [3], Olutola Adeyemo [4] and Damilola Adeniji [5]

[1] *Department of Neurosurgery, University of Texas, Houston, Texas, USA.*
[2] *Department of Biochemistry, University of Ibadan, Ibadan, Oyo state, Nigeria.*
[3] *Department of Pharmaceutical Engineering and Technology, India Institute of Technology, Varanasi, Uttar Pradesh, India.*
[4] *Department of Gynecology and Obstetrics, Federal Teaching Hospital Ido-Ekiti, Ekiti State, Nigeria.*
[5] *Department of Science Laboratory Technology, Federal Polytechnic, Ado-Ekiti, Ekiti- state, Nigeria*

World Journal of Advanced Research and Reviews, 2024, 23(01), 1419–1435

Publication history: Received on 08 June 2024; revised on 15 July 2024; accepted on 17 July 2024

Article DOI: https://doi.org/10.30574/wjarr.2024.23.1.2130

Abstract

Several of the bacteria responsible for pneumonia had become resistant to available antibiotics. According to the WHO, the resistance of *Klebsiella pneumonia* to Ciprofloxacin is 79.4%, making infections such as pneumonia and several diseases more difficult, if not impossible to treat. The prevalence of antimicrobial resistance is a global problem and among the 10 top global health threats facing humanity. With the projection of 10 million deaths per year by 2050 due to bacterial infections associated with antibiotic resistance according to WHO, there is an urgent need to identify an alternative approach to curb the incessant antimicrobial resistance and a complementary approach is to employ the use of naturally occurring compounds with potent antibacterial activities. We employed structural bioinformatics and theoretical chemistry techniques via molecular docking, and pharmacokinetic study, to identify novel *S. pneumoniae* topoisomerase IV inhibitors. The stringent molecular docking identified Arg140, Arg81, Glu55, Pro84, Met83, and Asn51, as principal amino acid residues for topoisomerase IV ligand interactions. Ten of the bioactive compounds found in *Vernonia amygdalina* showed a higher binding energy when compared to the reference compound (Ciprofloxacin). The overall analysis of MD results and binding free energy calculations reveal that Luteolin and 7-O-methylwogonin displayed stable trajectories with acceptable RMSD values and sufficient high negative energies throughout the MD simulation run of 100ns. These identified bioactive compounds in this study can be taken further for in vitro and In vivo studies to examine their efficacy against Pneumonia.

Keywords: Pneumonia; Molecular dynamic simulations; Luteolin; 7-O Methylwogonin; Ciprofloxacin

1. Introduction

Lower respiratory tract infections including pneumonia have been shown to affect 489 million people according to 2019 data from Global Burden of Disease (GBD) (1). Pneumonia is an acute respiratory infection that affects the distal bronchial tree and alveoli where the exchange of oxygen and carbon dioxide takes place. It's divided into hospital-acquired pneumonia and community-acquired pneumonia (2). The population most affected by pneumonia according to the 2019 GBD study is children under 5 years and adults above 70 years of age (3). The microorganisms responsible for Community-acquired pneumonia (CAP) and Hospital-acquired pneumonia (HAP) are different such that *streptococcus pneumonia*, *mycoplasma pneumonia, klebsiella pneumonia, legionella pneumonia,* and respiratory viruses are responsible for CAP while *staphylococcus aureus*, non-fermenting gram-negative bacilli and enterobacterales are responsible for HAP (4,5). Aspiration pneumonia constitutes 5-15% of community-acquired pneumonia cases, and the lack of robust diagnostic tools has made it a true burden (6). Several of the bacteria responsible for pneumonia had

* Corresponding author: Ayobami Fidelix

become resistant to available antibiotics. According to the WHO, the resistance of *Klebsiella pneumonia* to Ciprofloxacin is 79.4%, making infections such as pneumonia and several diseases more difficult, if not impossible to treat (7).

The emergence of new antibiotic-resistant mechanisms has spread internationally, pulling the treatment of prevalent infectious diseases in jeopardy as it's well known that bacterial infections are one of the leading causes of mortality and illnesses (8). The prevalence of antimicrobial resistance is a global problem and among the 10 top global health threats facing humanity (9), we are approaching a post-antibiotic era in which minor injury and common infections can kill again if proactive actions are not taken. Also, the pandemic of coronavirus diseases 2019 (COVID-19) has not helped as it has been reported that COVID-19 worsens antibiotic resistance (10).

The use of serotype replacement has complicated the use of vaccines for the treatment of bacterial infections, underlining the need for an alternate approach to combating emerging antimicrobial resistance (11). With the projection of 10 million deaths per year by 2050 due to bacterial infections associated with antibiotic resistance according to WHO (12), there is an urgent need to identify an alternative approach to curb the incessant antimicrobial resistance and a complementary approach is to employ the use of naturally occurring compounds with potent antibacterial activities (13-15). The naturally occurring bioactive compound exerts their mechanism of action through different mechanisms among which is the damage of DNA and intracytoplasmic component of the bacterial, alteration of the cell wall and cell membrane (16-17).

Vernonia amygdalina is a small shrub perennial plant of 1m -6m in height (18). It's most fondly called bitter leaf because of the bitter taste which has been attributed to the presence of bioactive compounds such as glycosides, tannins, saponins, etc. The bitter taste made them act as a substitute for hop in beer brewing without reducing the quality of the malt (19). The presence of its diverse bioactive compounds is responsible for their various pharmacological properties such as antimicrobial, anti-inflammatory, antibacterial, anti-fungi, anti-cancer, etc. (20, 21).

Here, we investigated the therapeutic potential of the bioactive compounds from *Vernonia amgydalina* in the treatment and management of pneumonia using in silico study. Also, the ADMET profiling and drug-likeness of the identified bioactive compound are justified via molecular docking tools.

2. Material and methods

2.1. Protein Preparation

The Crystal structure of *S. pneumoniae* DNA topoisomerase IV complexed with ATP inhibitor was obtained from the Protein Data Bank (PDB) (https://www.rcsb.org/) in PDB format (PDB: 4EM7) with a crystallographic resolution of 1.90 Å. UCSF Chimera Software (v 1.16) was used to minimize and prepare the target protein. The prediction of binding sites of protein was made through BIOVIA Discovery Studio, additionally, with the help of the online Platform CASTp (http://sts.bioe.uic.edu) (22).

2.2. Ligands preparation

Fifty-six phytochemicals from *Vernonia Amygdalina* were sought from published literature (23-25), the chemical, structural details and canonical SMILES of the phytochemicals were obtained from PubChem database (https://pubchem.ncbi.nlm.nih.gov/). The 2D structures of the phytochemicals and the reference drug (ciprofloxacin) were downloaded in SDF format. Using Discovery Studio, the SDF structures were saved in PDB format.

2.3. Molecular Docking Analysis

Molecular docking analysis and binding affinities were done with the tool known as Auto Dock Tools 4.2 (26). Pdbqt format of the different protein targets and ligands were dragged into their respective columns. All the ligands were docked, and a maximum of 8 exhaustiveness was computed for all of them. All other parameters in the software were in default mode. The binding affinities of compounds for the protein targets were recorded. The compounds were then ranked by their affinity scores. Also, the molecular interactions between protein targets and the compounds were viewed with BIOVIA Discovery Studio. Amino acids engaging with the ligand, hydrogen bonds (H-bonds), hydrophobic interaction, and the individual atoms involved were examined in each ligand cluster.

Table 1 The grid center, the dimensions of each target protein, and the amino acid residue present at the active site

Protein targets	Grid centers	Dimension of the grid box	Amino acid at the active sites
Topoisomerase IV	x = 13.4937	x = 19.5221	Arg140, Arg81, Glu55, Pro84, Met83, Asn51.
	y = 32.5629	y = 18.8575	
	z = 8.4658	z = 23.2677	

2.4. In silico study

The ranking of protein–ligand complexes was conducted based on the docking score (binding energy). When the binding energy is <5kcal/mol, the receptor and ligand have a relatively good binding property. The Docking Scores of some bioactive compounds from *Vernonia amygdalina* against Topoisomerase IV are shown in Table 2

Table 2 The Docking Scores of the top 10 bioactive compounds from *Vernonia amygdalina* with the best binding affinity for Topoisomerase IV

S/N	Compounds	Docking Score
1	7-O-Methylwogonin	-7.9
2	Dihydroskullcapflavone	-7.6
3	Luteolin	-7.7
4	Luteolin-7-glucuronide	-7.6
5	Andrographolactone	-7.5
6	Apigenin	-7.4
7	Baicaline	-8.4
8	Rhoifolin	-7.5
9	Vernoniosides A1	-7.5
10	4-Methylumbelliferyl	-7.8
11	Ciprofloxacin	-7.3

2.5. Druglikeness of bioactive compounds

Table 3 below shows the drug-likeness properties of the top ten *Vernonia amgydalina* bioactive compounds with the best binding affinity. The bioactive compounds were subjected to Lipinski's rule, Muegge's rule, Ghose's rule, Verber's rule, and Egan's rule. Also, the analysis of the bioavailability score was carried out for each bioactive compound. This was carried out using the SwissAdme online website (27).

Table 3 The druglikeness of the top 10 bioactive compounds with the best binding affinity for Topoisomerase IV

No	Compounds	M/W g/mol	Lipinski violation	Ghose violation	Veber Violation	Egan Violation	Muegge Violation	Bioavailability score
1	7-O methylwogonin	298.29	0	0	0	0	0	0.55
2	Luteolin	286.24	0	0	0	0	0	0.55
3	Di-hydroskullcupflavone	316.31	0	0	0	0	0	0.55
4	Andrographolactone	296.40	1	0	0	0	0	0.55
5	Apigenin	270.24	0	0	0	0	0	0.55
6	4-Methylumbelliferyl	160.17	0	0	0	0	1	0.55
7	Rhoifolin	578.52	3	4	1	1	3	0.17
8	Vernoniosides A1	66.78	3	3	1	1	5	0.17
9	Baicalin	446.36	2	0	1	1	3	0.11
10	Luteolin-7-glucoronide	462.36	2	0	1	1	3	0.11

2.6. Binding modes and molecular interactions

The binding mode and the nature of intermolecular interactions provide crucial insights into mode of interaction between the selected compounds and the target protein. These interactions are essential for determining the stability and affinity of a compound within the active site of a specific protein.

Upon visualization, the predominant molecular interactions observed with 7-O-methylwogonin, Dihydroskullcapflavone, Andrographolactone, Luteolin, Apigenin, 4-methylumbelliferyl, and Ciprofloxacin primarily involved hydrogen bonding and pi-interactions with the binding sites of Topoisomerase IV (Figure 1A-G). Specifically, hydrogen bonds were identified between the atoms of 7-O-methylwogonin and the side chain of Gly82, between the atoms of Dihydroskullcapflavone and the side chain of Arg81, and between the atoms of Andrographolactone and the side chain of Asn51. Luteolin demonstrated interactions with side chains Asn51, Val76, and Ser124 via hydrogen bonding. Similarly, hydrogen bond interactions were established between the side chains of Asn51 and Ser124 and the atoms of Apigenin. In addition, the atoms of 4-methylumbelliferyl interacted with the side chains of Arg81, Ser124, Asn51, and Met83 via hydrogen bonds. Ciprofloxacin was found to interact with the side chains of Asp78 and Thr172.

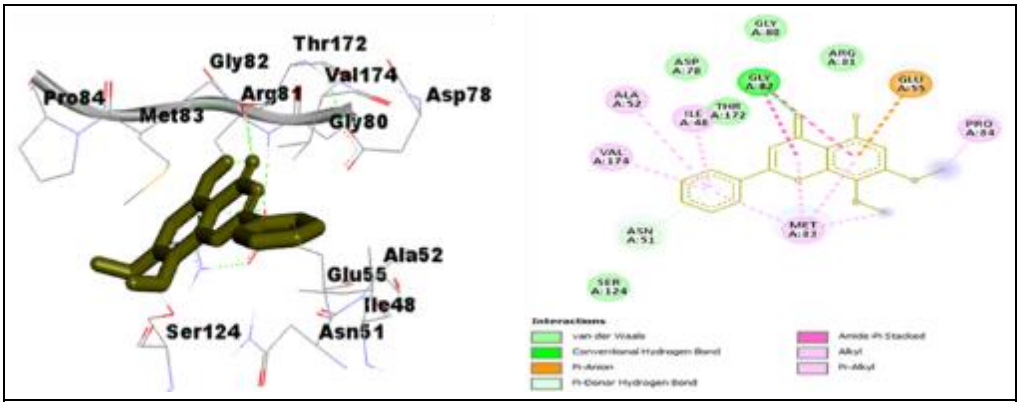
Thr172
Gly82
Val174
Pro84
Arg81
Asp78
Met83
Gly80
Ala52
Glu55
Ile48
Ser124
Asn51

A

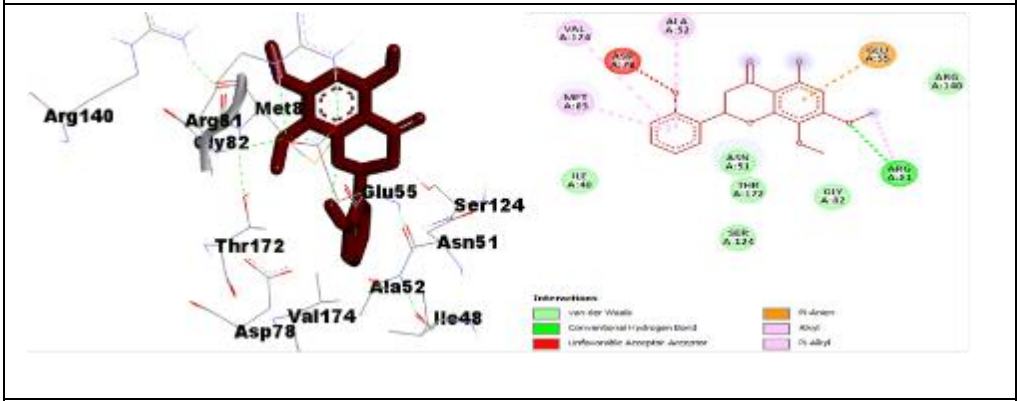
Arg140
Arg81
Met8
Gly82
Glu55
Ser124
Thr172
Asn51
Ala52
Val174
Ile48
Asp78

B

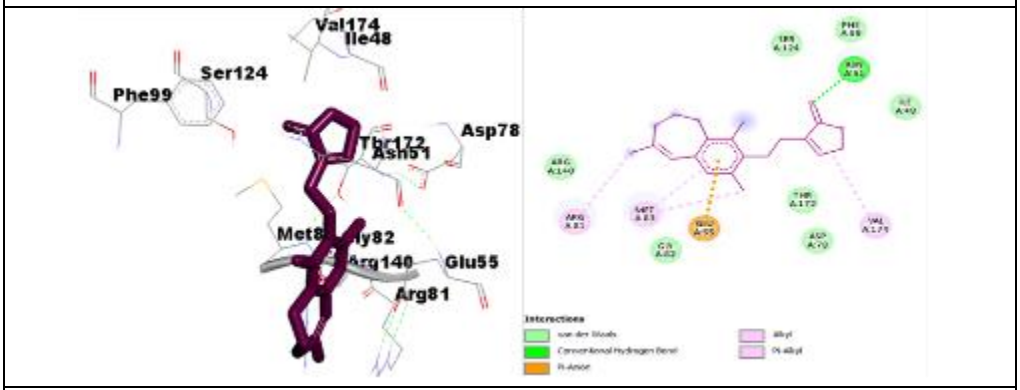
Val174
Ile48
Ser124
Phe99
Asp78
Thr172
Asn51
Met8
Gly82
Arg140
Glu55
Arg81

C

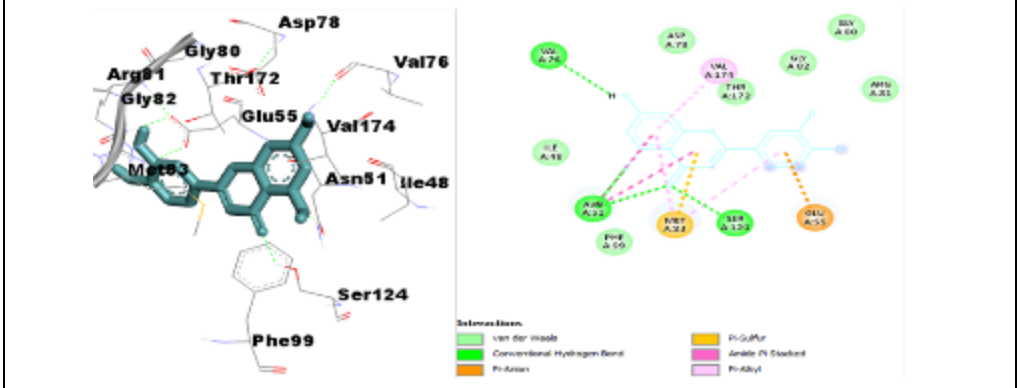
Asp78
Gly80
Val76
Arg81
Thr172
Gly82
Glu55
Val174
Met83
Asn51
Ile48
Ser124
Phe99

D

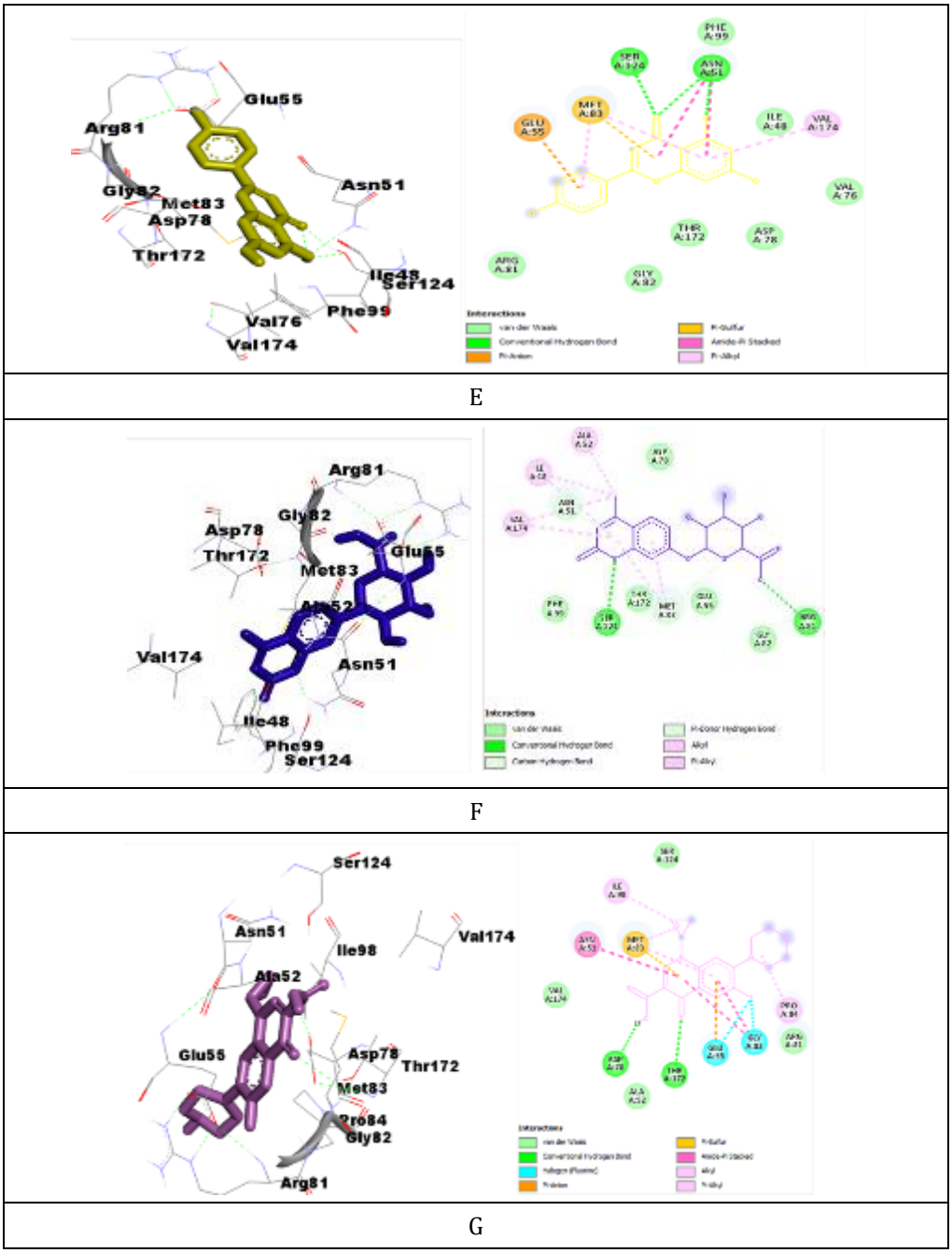

Figure 1 Binding interaction of Topoisomerase IV with a) 7-O-methylwogonin b) Dihydroskullcapflavone c) Andrographolactone d) Luteolin e) Apigenin f) 4-methylumbelliferyl g) Ciprofloxacin

2.7. ADMET Properties

The ADMET properties are used in the prediction of the pharmacokinetics potentials of the bioactive molecules (28). The ADMET result was analyzed using the ADMETSLAB 2.0 web server (29). The knowledge of the pharmacokinetics of bioactive compounds is suitable for the determination of compounds suitable for oral dosing, assuming the intestinal permeability, blood-brain barrier permeability, hepatotoxicity, and many more.

Table 4 ADME prediction table

	Compounds					
ABSORPTION	**4 Methyl umbelliferyl**	**7-O-Methyl Wogonin**	**Dihydroskull-capflavone**	**Apigenin**	**Luteolin**	**Andrographolactone**
Caco-2 Permeability	+	+	+	+	-	+
Pgp-inhibitor	+	-	+	+	+	+
Pgp-substrate	+	+	+	+	+	+
Human intestinal absorption (HIA)	+	+	+	+	+	+
DISTRIBUTION						
Plasma protein binding (PPB)	95.978%	97.55%	95.029%	96.535%	97.642%	98.612
Volume of distribution (Vd)	-0.501	0.261	-0.116	-0.463	-0.614	0.428
Blood-brain barrier (BBB)	+	+	+	+	+	-
METABOLISM						
CYP1A2 inhibitor	-	+	+	-	-	-
CYP1A2 substrate	-	-	-	+	+	-
CYP2C19 inhibitor	+	-	-	+	+	-
CYP2C19 substrate	+	+	+	+	+	-
CYP2C9 inhibitor	+	-	-	+	+	+
CYP2C9 substrate	-	+	+	+	+	-
CYP2D6 inhibitor	+	+	+	-	+	+
CYP2D6 substrate	+	+	+	-	-	+
CYP3A4 inhibitor	+	-	+	-	-	-
CYP3A4 substrate	-	+	-	+	+	-
EXCRETION						
Clearance	6.591	6.213	5.473	5.939	8.482	7.945
T1/2	1.19	1.047	1.22	1.203	1.373	0.615
TOXICITY						
hERG Blockers	-	-	-	-	-	-
AMES Toxicity	+	-	+	+	+	-
Skin Sensitization	-	-	-	+	-	-
Carcinogenicity	+	+	+	-	+	-
Human hepatotoxicity	+	-	-	+	+	+
Drug-induced Nephrotoxicity	+	+	_	+	+	+

2.8. Molecular dynamics (MD) simulation studies

MD simulation studies for the top selected protein-ligand complexes were carried out with GROMACS 2020 package using the CHARMM-36M force field (30). The best docking conformation with the least binding energy (most negative) was selected as the initial conformation for the MD run. The topology files for the individual ligands from their respective complexes were generated using the CHARMM-GUI web server (31). The TIP3P model was used to solvate the complexes and apply periodic boundary conditions across all directions. The excessive charge present on the complexes was neutralized by adding the calculated number of Na+ and Cl- ions using the Monte Carlo ion placing method. Further, complexes were energy minimized for 5000 steps of the steepest descent algorithm. All the hydrogen bonds present were constrained through the LINCS algorithm (32). Later, the systems were equilibrated with NVT and NPT ensembles for 1ns using the leap-frog integrator. Once the equilibration was done, the systems were subjected to isobaric and isothermally controlled MD production of 100 ns. The normal temperature (310.15 K) and pressure (1 bar) conditions were monitored throughout the MD simulation using velocity-rescaling and Parrinello-Rahman pressure methods, respectively.

After the completion of MD production run, the obtained MD trajectories for individual complexes were structurally and conformationally analyzed based on RMSD, RMSF, inter-hydrogen bond, SASA, and Rg values calculated using inbuilt modules of GROMACS 2020 viz. gmx_rms, gmx_rmsf, gmx_hbond, gmx_sasa, and gmx_gyrate respectively. All MD plots described in the study were generated using the QtGrace tool (33, 34).

2.9. Binding free energy calculations (MMPBSA assay)

In structure-based drug designing, it is crucial to analyze binding affinity between ligand and receptor proteins. MMPBSA assay (Molecular Mechanics Poisson Boltzmann Surface Area) is the most versatile computational technique for endpoint binding free energy calculations of non-covalently interacting protein-ligand systems. Theoretically, a system's net binding free energy (ΔGbind) is estimated by deducting individual receptor and ligand energy from the total energy associated with the complex (35).

$$\boldsymbol{\Delta G_{bind}} = \boldsymbol{\Delta G_{complex}} - \boldsymbol{\Delta G_{protein}} - \boldsymbol{\Delta G_{ligand}} \dots\dots\dots (1)$$

Also, ΔG_{bind} is expressed as a function of enthalpy of binding (ΔH) and conformational entropy (ΔS) (after binding of ligand to the receptor) at a specified temperature (T).

$$\boldsymbol{\Delta G_{bind}} = \boldsymbol{\Delta H - T\Delta S} \dots\dots\dots (\mathbf{2})$$

ΔH is the net contribution of changes in solvation (polar and non-polar) and mechanical energy (bonding and non-bonding) during protein-ligand interaction (**equation 3**). Further, entropy changes (translational, rotational, and vibrational) are estimated using statistical calculations based on normal mode analysis (NMODE) and quasi-harmonic (QH) approximation.

$$\boldsymbol{\Delta H} = \boldsymbol{\Delta E_{MM}} + \boldsymbol{\Delta G_{sol}} \dots\dots\dots (\mathbf{3}$$

Where

$$\boldsymbol{\Delta E_{MM}} = \boldsymbol{\Delta E_{bonded}} + \boldsymbol{\Delta E_{non-bonded}} = \left(\boldsymbol{\Delta E_{bond}} + \boldsymbol{\Delta E_{angle}} + \boldsymbol{\Delta E_{dihedral}}\right) + \left(\boldsymbol{\Delta E_{ele}} + \boldsymbol{\Delta E_{vdwaals}}\right) \dots\dots\dots (\quad)\mathbf{4}$$

And

$$\boldsymbol{\Delta G_{sol}} = \boldsymbol{\Delta G_{polar}} + \boldsymbol{\Delta G_{non-polar}} = \boldsymbol{\Delta G_{PB/GB}} + \boldsymbol{\Delta G_{non-polar}} \dots\dots\dots (\mathbf{5})$$

The non-polar component described in **equation 5** is correlated to solvent accessible surface area (SASA) of the complex through an experimentally calculated numerical value based on solvation energy of non-polar molecules.

$$\boldsymbol{\Delta G_{non-polar}} = \boldsymbol{NP_{tension}\, X\, \Delta SASA} + \boldsymbol{NP_{offset}} \dots\dots (\mathbf{6})$$

Or

$$\boldsymbol{\Delta G_{non-polar}} = \boldsymbol{\Delta G_{disp.}} + \boldsymbol{\Delta G_{cavity}} = \boldsymbol{\Delta G_{disp.}} + \left(\boldsymbol{cavity_{tension}\, X\, \Delta SASA} + \boldsymbol{cavity_{offset}}\right) \dots\dots\dots (\mathbf{7})$$

In the current study, the gmx_MMPBSA tool was utilized to perform end-state free energy calculations (ΔGbind) for the selected protein-ligand complexes. This tool is written in Python 3.8 and combines the functionality of GROMACS and Amber to generate input files for necessary calculations at the interface of the Miniconda environment. The complexes were simulated for 100ns under normal physiological conditions, viz. 310.15 K temperature and 1 bar pressure using GROMACS 2020. The MD trajectory file, topology file, and index file generated were deployed to calculate binding free energy (36).

3. Results and discussion

3.1. Druglikeness/ADMET

Lipinski's rule of five, Ghose's, Veber's, Egan's and the Muegge's rule were used for the assessment of the top ten bioactive compounds. Table 3 shows the predicted druglikeness and the molecular weight of each compound which is a major determinant if a drug can be taken orally or not. Of the top ten bioactive compounds, 7-O methylwogonin, luteolin, dihydroskullcupflavone and Apigenin don't have any violation of the five rules listed above. Andrographolactone and 4 methylumberriferyl has a violation in Lipinski rule of five and Muegge's violation respectively. The remaining bioactive compounds viz Baicalin, Luteolin-7-glucoronide, Rhoifolin and Vernoniosides A1 have variable number of violations of all the five rule as shown in table 3.

The absorption of chemicals, its distribution, metabolism, excretion, and toxicity (ADMET) are the five major properties that need to be put into consideration during drug discovery (37). The prediction of the ADMET properties of these bioactive compounds plays a significant role such that a drug with poor ADMET properties account for the failure of several drugs when subject to the clinical trials. A good drug candidate should be absorbed adequately into the body system for effective metabolism and action. Table 4 shows the results of the ADMET studies performed on the top six compounds. The six selected compounds as shown in Table 4 had excellent intestinal absorption, which is an important requirement for a drug since the primary site responsible for absorption is the intestine (38). Of the six compounds, five of them display high Caco2 permeability, which is good for the study of the invitro mode of the intestinal mucosa. The six selected compound in exception of 7-O methylwogonin were found to P-glycoprotein inhibitor, making it more pharmacologically active than non-inhibitors and all the six bioactive compounds are substrates of P-glycoprotein, an efflux membrane transporter responsible for the distribution of xenobiotics (39). Also, all the six selected compounds had a low VDss value, indicating that more of the compound would be distributed in the plasma rather than the tissue and they have a high half-life in terms of total clearance, suggesting that they aren't rapidly cleared from the body (40). The six selected compounds are inhibitors of CYPIA2 except 7-O methylwogonin and Dihydroskullcapflavone. besides, all these compounds are inhibitors of CYP2D6 except Apigenin. All the six compounds are not hERG I inhibitors, thus this reduces the risk of cardiotoxic side effects during clinical trials.

3.2. Molecular dynamics (MD) simulations study

The MD simulation studies aid in an in-depth understanding of structural and conformational changes occurring in the system under a controlled simulated physiological environment. Moreover, the effects of solvation and surrounding ions on binding interactions between protein and ligand can be better identified through the studies. To establish the stability, the best-docked conformation of the top six ligands (**Andrographolactone**, **Apigenin**, **Ciprofloxacin**, **Dihydroskullcapflavone**, **Luteolin**, and **7-O-methylwogonin**) complexed with the protein were selected and subjected to MD simulation run of 100 ns using GROMACS 2020. Further, different parameters such as RMSD, RMSF, Rg, SASA, H-BOND, and PCA were studied to understand the pattern and overall stability of the complexes.

3.2.1. RMSD analysis

The root mean square deviation (RMSD) is a vital parameter to elucidate the protein's stability based on conformational changes in the protein backbone from its initial to final pose. The lesser the deviation, the better the complex stability throughout the run. The RMSD value was calculated using equation 8 (41).

$$\boldsymbol{RMSD_x} = \sqrt{\frac{1}{N}\sum_{i=1}^{N}(\boldsymbol{r_i'(t_x)} - \boldsymbol{r_i(t_{ref})})^2} \ldots\ldots\ldots\ldots (\mathbf{8})$$

Where N is the total number of atoms in the selection, t_{ref} is the reference time for the first frame taken as the reference at time $t=0$, t_x denotes the recording time for frame x, and r' indicates the position of the selected atoms after superimposing frame x on the reference frame.

The average RMSD value for the protein-ligand complexes of Andrographolactone, Apigenin, Ciprofloxacin, Dihydroskullcapflavone, Luteolin, and 7-O-methylwogonin was found to be 0.48, 0.29, 0.69, 2.17, 0.20, and 0.14 nm, respectively. All the ligands had acceptable RMSD values within 1nm (except Dihydroskullcapflavone), depicting their stability during the MD simulations run (Figure 2 and Figure 3). However, only two ligands (Luteolin and 7-O-methylwogonin) displayed overall stable trajectories throughout the simulation run of 100 ns.

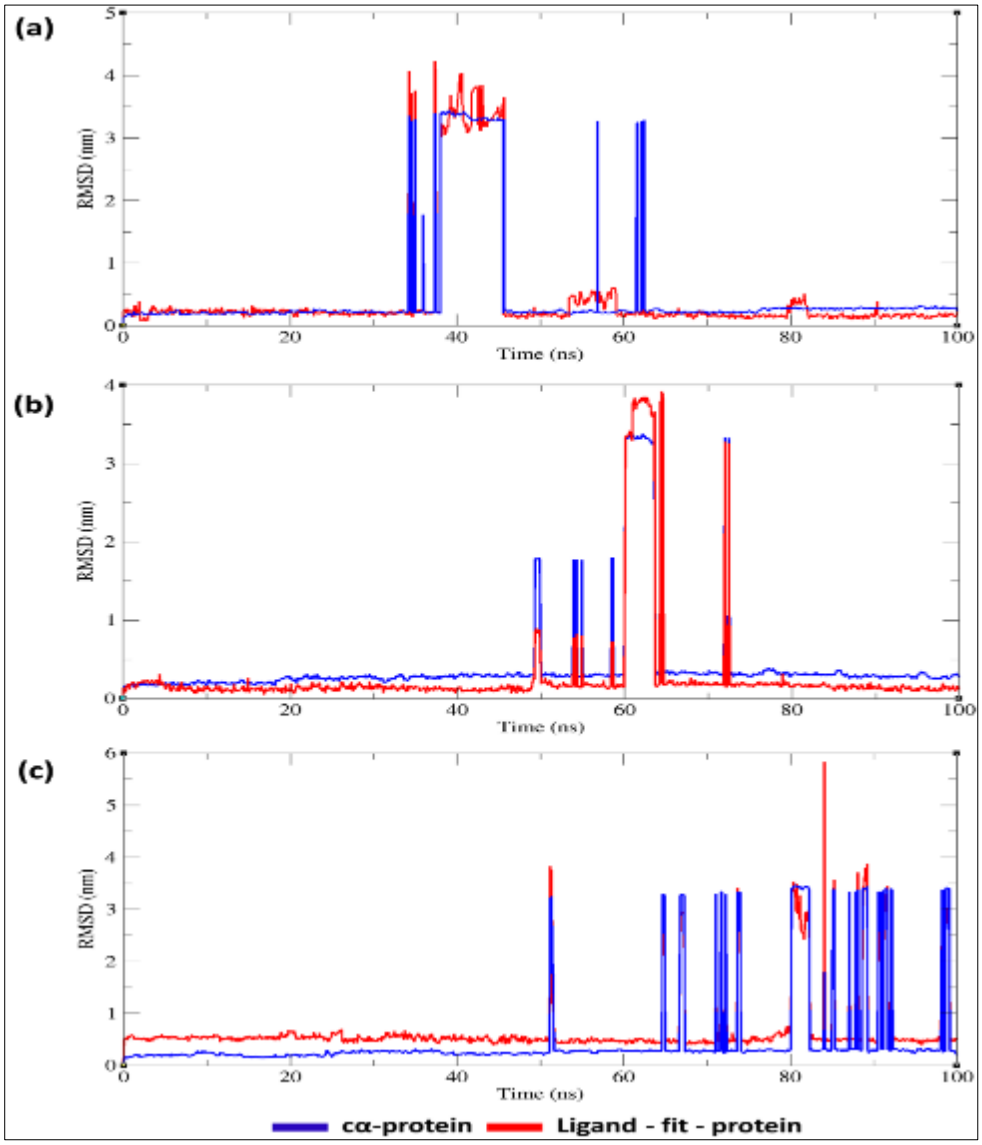

Figure 2 RMSD plot of the selected ligands in complex with the protein: (a) Andrographolactone, (b) Apigenin, and (c) Ciprofloxacin

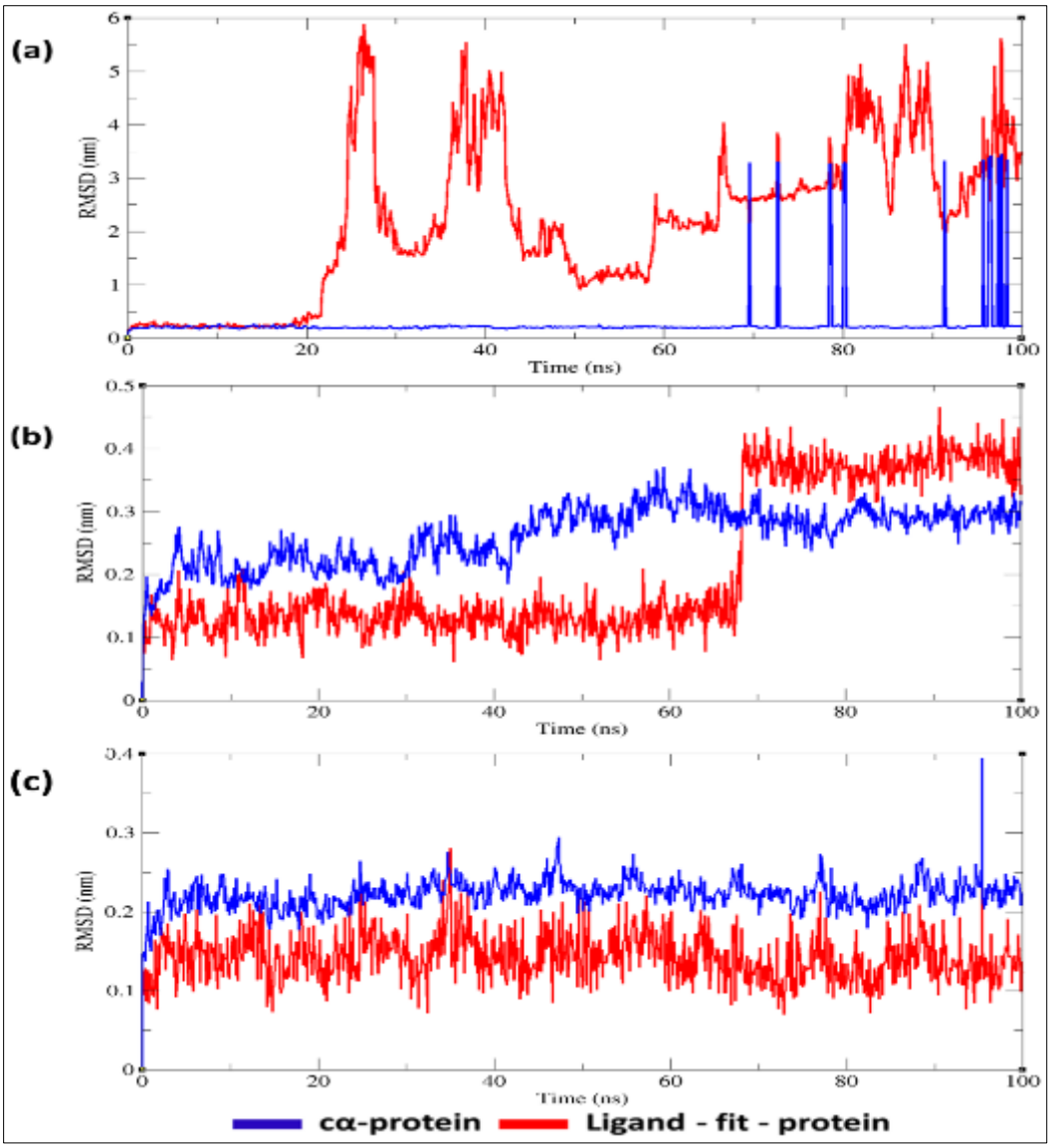

Figure 3 RMSD plot of the selected ligands in complex with the protein: (a) Dihydroskullcapflavone, (b) Luteolin, and (c) 7-O-methylwogonin

3.2.2. RMSF analysis

The root mean square fluctuation (RMSF) value is the indirect measure of the stiffness and flexibility of protein chains. It is an important parameter to identify the least stable regions of a protein molecule that may alter the binding pattern of the ligand to its binding pocket. The peaks observed in a typical RMSF plot correspond to the most oscillating residues. Proteins with large flexible domains have higher RMSF values. The RMSF value for the selected protein-ligand complexes was calculated based on the data generated from MD trajectories using equation 9 (42).

$$\boldsymbol{RMSF_i} = \sqrt{\frac{1}{T}\sum_{t=1}^{T} < (r_i'(t) - r_i(t_{ref}))^2 >} \quad \ldots\ldots\ldots\ldots\ldots\ldots (9)$$

Where T indicates trajectory time, t_{ref} denotes the reference time, r_i represents *the* i_{th} residue position, and r_i' corresponds to the atomic position of *the* i_{th} residue obtained after overlaying on the reference.

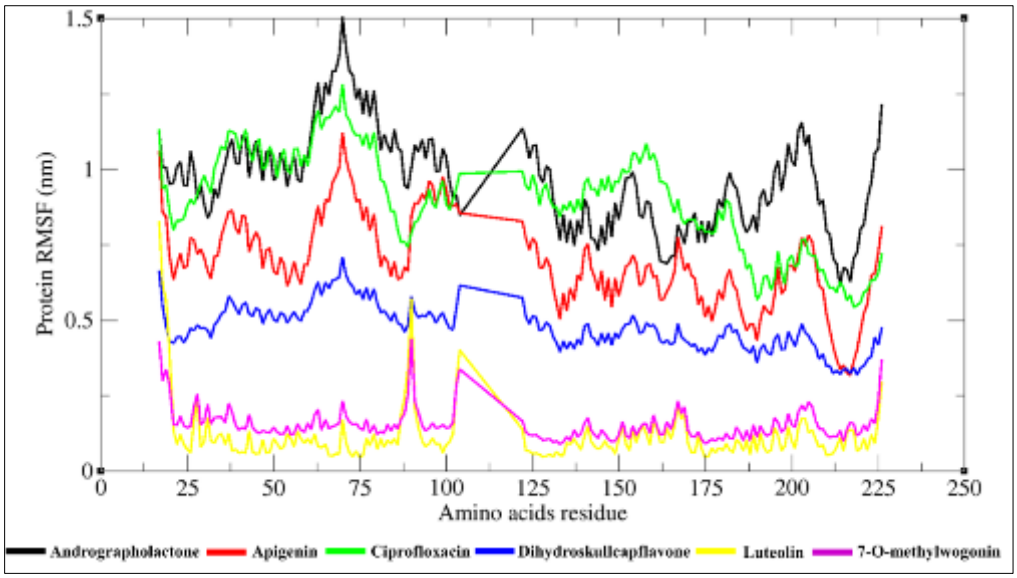

Figure 4 RMSF plot

The angle brackets in the equation denote the average taken for the square distance calculated for the protein's residue atoms. The average RMSF value for the selected protein-ligand complexes of Andrographolactone, Apigenin, Ciprofloxacin, Dihydroskullcapflavone, Luteolin, and 7-O-methylwogonin was found to be 0.96, 0.69, 0.89, 0.47, 0.11, and 0.15 nm, respectively indicating the stability of the complexes formed (Figure 4).

3.2.3. Radius of gyration (Rg) analysis

The value of the radius of gyration (Rg) gives an idea about the size, compactness, flexibility, and folding/unfolding of the protein molecules. The Rg was determined for each protein-ligand complex utilizing the data generated from the MD simulation run (equation 10).

$$\boldsymbol{RoG} = \sqrt{\frac{\mathbf{1}}{\boldsymbol{N}}\sum_{\boldsymbol{i=1}}^{\boldsymbol{N}}|\boldsymbol{r_i} - \boldsymbol{r_{center}}|^2} \ldots\ldots (\mathbf{10})$$

Where r_i and r_{center} correspond to atom coordinates and center of mass, respectively. N denotes the number of atoms in the protein. The protein systems with lower Rg values are considered stiffer and more compact (43).

The average Rg value for Andrographolactone, Apigenin, Ciprofloxacin, Dihydroskullcapflavone, Luteolin, and 7-O-methylwogonin-protein complexes was calculated to be 1.815, 1.747, 1.797, 1.715, 1.662, and 1.663 nm respectively (Figure 5). The overall values of Rg for Luteolin and 7-O-methylwogonin-protein complexes remained nearly constant throughout the MD simulations.

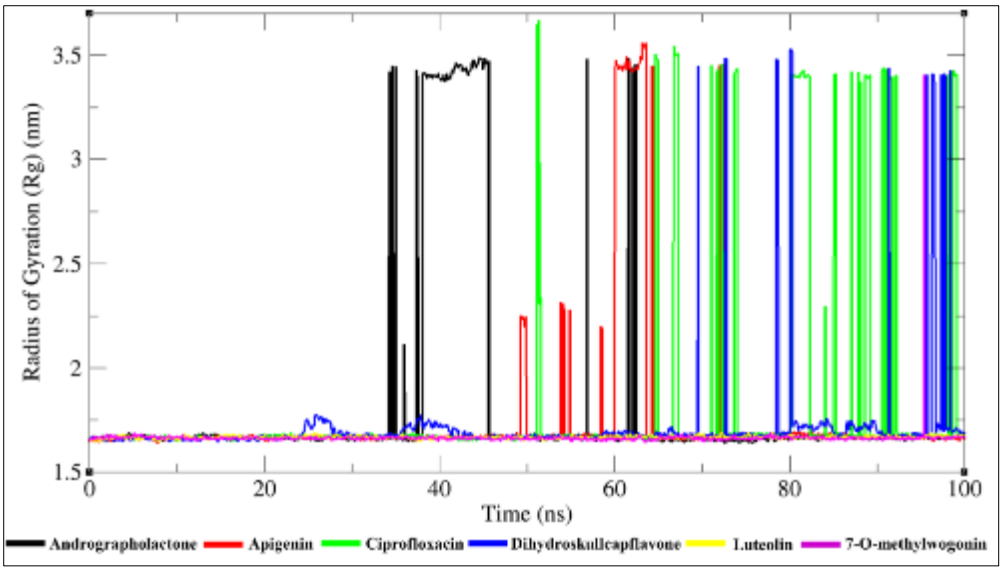

Figure 5 Rg plot

3.2.4. Solvent accessible surface area (SASA) analysis

The SASA value for a biomolecule reflects its rigidity and compactness. It is defined as the surface area of a macromolecule which solvent molecules can access through van der Waals forces. The SASA is determined by imagining the molecular surface as a collection of dots and then tracing the accessible surface area with a probe, typically a sphere. The systems with lower SASA values are considerably more rigid and compact (44). The average value of SASA for protein-ligand complexes of Andrographolactone, Apigenin, Ciprofloxacin, Dihydroskullcapflavone, Luteolin, and 7-O-methylwogonin was found to be 103.73, 104.91, 105.17, 103.85, 104.28, and 103.58 nm^2 respectively (Figure 6).

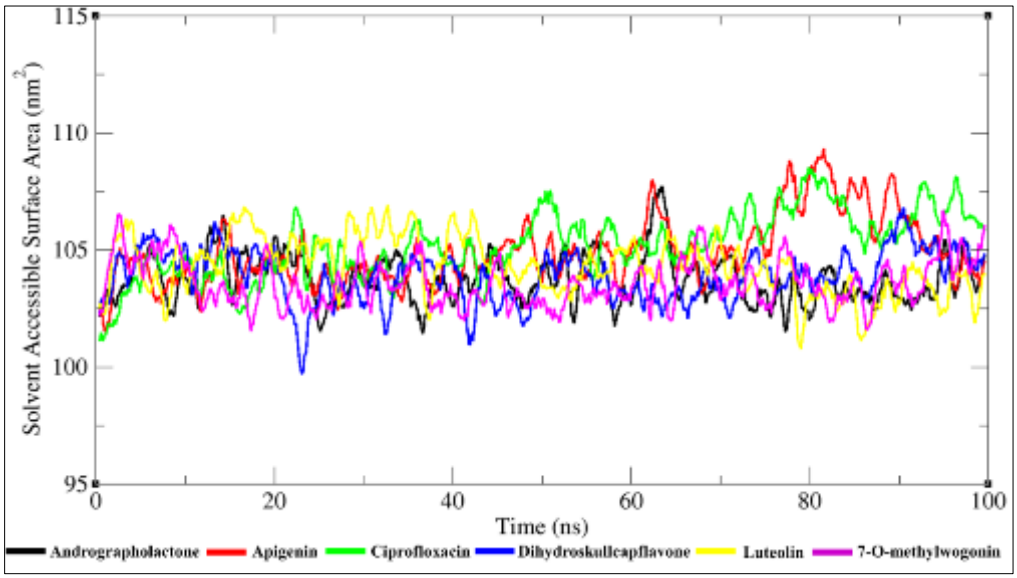

Figure 6 SASA plot

3.2.5. H-bond analysis

The hydrogen bond is the most characteristic interaction between the protein and the ligand that governs the overall stabilization of the complex formed. Further, it also affects the pharmacokinetic properties of the ligand, viz. absorption, distribution, metabolism, and excretion. The number of hydrogen bonds formed between protein and ligand complexes was analyzed during MD simulations (45).

The ligand Andrographolactone formed a maximum of three hydrogen bonds with the target protein; however, slight fluctuations and deviations in the total number of bonds were observed during the initial 50 ns of MD simulations as depicted in its hydrogen bond graph (Figure 7). While the ligands Apigenin, Ciprofloxacin, Dihydroskullcapflavone, Luteolin, and 7-O-methylwogonin formed an average of four, six, three, four, and two H-bonds with the target protein, respectively. The hydrogen-bond distribution as a function of donor-acceptor distance for each ligand has been depicted in Figure 7.

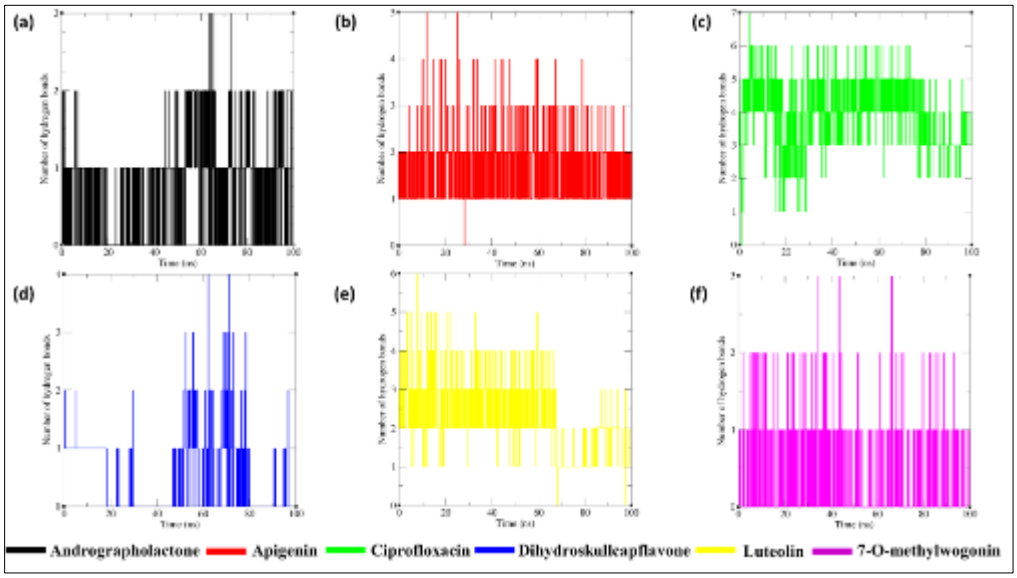

Figure 7 Graphs depicting the number of intermolecular H-bonds formed between protein-ligand complexes

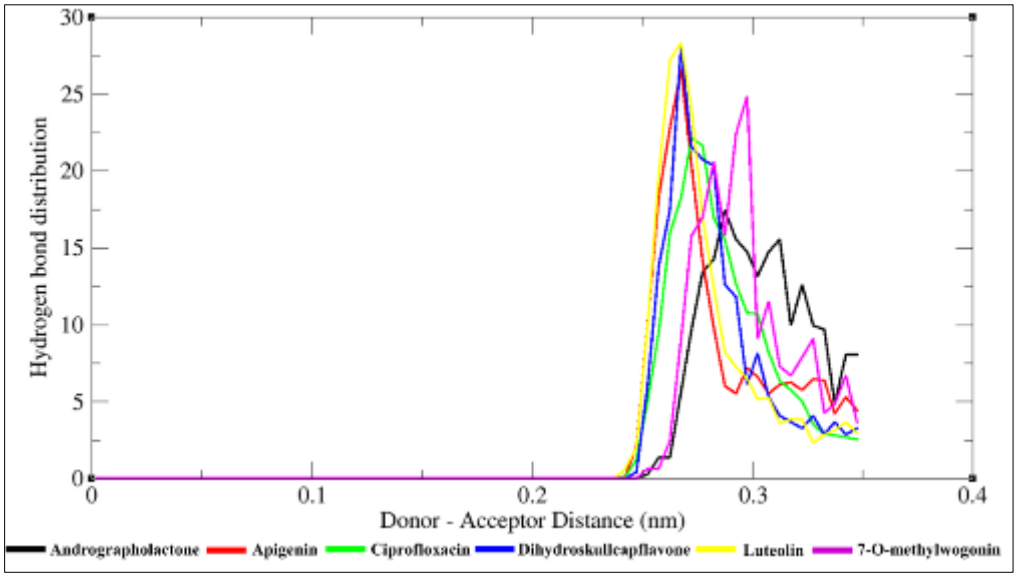

Figure 8 H-bond distribution (within 0.3nm distance) for protein-ligand complexes

3.3. Binding free energy calculations

The analysis of ligands based on end-state binding free energy is of great significance over simple docking scores generated using molecular docking. It provides a clear-cut idea about the atomistic level interactions occurring between protein and ligand responsible for the ligand's affinity towards the protein. The binding free energy calculations for the selected ligands were carried out by considering molecular mechanical energies and solvation energies associated with their complexes. Ligands were analyzed based on their determined net binding free energy (ΔG_{total}).

All ligands except Dihydroskullcapflavone displayed significantly higher negative free energy values, indicating overall stable binding interactions between protein and ligand. The data corresponding to the contribution of different energies

associated with protein-ligand interaction in the gas phase (electrostatic, van der Waals) and solvation phase (polar, non-polar) for different ligands have been summarized in Table 5.

Table 5 Energy contributions of different protein-ligand complexes in MMPBSA assay

S.No.	Compound ID	$\Delta G_{VDWaals}$ (kcal/mol)	ΔG_{EEL} (kcal/mol)	ΔG_{EPB} (kcal/mol)	$\Delta G_{ENPolar}$ (kcal/mol)	ΔG_{gas} (kcal/mol)	ΔG_{solv} (kcal/mol)	ΔG_{total} (kcal/mol)
1.	Andrographolactone	-33.68	-17.29	41.17	-3.58	-50.98	37.59	-13.39
3.	Apigenin	-31.13	-23.57	41.00	-3.14	-54.71	37.86	-16.85
2.	Ciprofloxacin	-20.16	-78.92	84.90	-3.18	-99.07	81.72	-17.35
4.	Dihydroskullcapflavone	-13.24	-10.99	19.31	-1.62	-24.23	17.69	-6.55
5.	Luteolin	-29.94	-35.84	48.45	-3.10	-65.79	45.36	-20.43
6.	7-O-methylwogonin	-37.26	-20.43	41.19	-3.23	-57.68	37.96	-19.73

Based on the overall analysis of MD results and binding free energy calculations, the protein-ligand complexes of ligands Luteolin and 7-O-methylwogonin displayed stable trajectories with acceptable RMSD values and sufficient high negative energies throughout the MD simulation run of 100ns.

4. Conclusion

The spread of antibiotic-resistant pathogens is causing major concern to the current global healthcare system and the only way out of this is through the discovery of potential novel drugs. This study identified hit compounds from *Vernonia amygdalina* that may be used for the inhibition of topoisomerase IV in pneumonia. The overall analysis of MD results and binding free energy calculations reveal that Luteolin and 7-O-methylwogonin displayed stable trajectories with acceptable RMSD values and sufficient high negative energies throughout the MD simulation run of 100ns.

Compliance with ethical standards

Disclosure of conflict of interest

No conflict of interest to be disclosed.

References

[1] Alara, O. R., Abdurahman, N. H., Mudalip, S. K. A., & Olalere, O. A. Phytochemical and pharmacological properties of Vernonia amygdalina. Journal of Chemical Engineering and Industrial Biotechnology, 2017; 2, 80-96.

[2] Cillóniz, C., Garcia-Vidal, C., Ceccato, A., & Torres, A. Antimicrobial resistance among Streptococcus pneumoniae. In I. W. Fong, D. Shlaes, & K. Drlica (Eds.), Antimicrobial Resistance in the 21st Century (2nd ed., pp. 13-38). Springer International Publishing AG. 2018

[3] Cillóniz, C., Ewig, S., Polverino, E., Marcos, M. A., Esquinas, C., Gabarrús, A., Mensa, J., & Torres, A. Microbial aetiology of community-acquired pneumonia and its relation to severity. Thorax, 2011; 66(4), 340-346.

[4] Daina, A., Michielin, O., & Zoete, V. SwissADME: A free web tool to evaluate pharmacokinetics, drug-likeness and medicinal chemistry friendliness of small molecules. Scientific Reports 2017; 7, 42717. https://doi.org/10.1038/srep42717

[5] Farombi, E. O., & Owoeye, O. Antioxidative and chemopreventive properties of Vernonia amygdalina and Garcinia biflavonoid. International Journal of Environmental Research and Public Health, 2017; 8(6), 2533-2555.

[6] GBD 2019 Diseases and Injuries Collaborators. Global burden of 369 diseases and injuries in 204 countries and territories, 1990-2019: A systematic analysis for the Global Burden of Disease Study 2019. The Lancet, 2020; 396(10258), 1204-1222.

[7] Khameneh, B., Iranshahy, M., Soheili, V., & Bazzaz, B. S. F. Review on plant antimicrobials: A mechanistic viewpoint. Antimicrobial Resistance & Infection Control, 2019; 8(1), 1-28.

[8] Mandell, L. A., & Niederman, M. S. Aspiration pneumonia. New England Journal of Medicine, 2019; 380(7), 651-663.

[9] Nwosu, S. I., Stanley, H. O., & Okerentugba, P. O. Occurrence, types and location of calcium oxalate crystals in Vernonia amydalina Del (Asteraceae). International Journal of Science and Nature, 2013; 4(3), 533-537.

[10] Strathdee, S. A., Davies, S. C., & Marcelin, J. R. Confronting antimicrobial resistance beyond the COVID-19 pandemic and the 2020 US election. The Lancet, 2020; 396(10257), 1050-1053.

[11] Torres, A., Cilloniz, C., Niederman, M. S., Menéndez, R., Chalmers, J. D., Wunderink, R. G., & van der Poll, T. Pneumonia. Nature Reviews Disease Primers, 2021; 7(1), 25. https://doi.org/10.1038/s41572-021-00259-0

[12] Torres, A., Niederman, M. S., Chastre, J., Ewig, S., Fernandez-Vandellos, P., Hanberger, H., Kollef, M., Li Bassi, G., Luna, C. M., Martin-Loeches, I., Paiva, J. A., Read, R. C., Rigau, D., Timsit, J. F., Welte, T., & Wunderink, R. International ERS/ESICM/ESCMID/ALAT guidelines for the management of hospital-acquired pneumonia and ventilator-associated pneumonia. European Respiratory Journal, 2017; 50(3), 1700582.

[13] Trott, O., & Olson, A. J. AutoDock Vina: Improving the speed and accuracy of docking with a new scoring function, efficient optimization, and multithreading. Journal of Computational Chemistry, 2010; 31(2), 455-461.

[14] Udochukwu, U., Omeje, F. I., Uloma, I. S., & Osiewe, F. D. Phytochemical analysis of Vernonia amygdalina and Ocimum gratissimum extracts and their antibacterial activities on some drug-resistant bacteria. American Journal of Research Communication, 2015; 3(5), 225-235.

[15] World Health Organization. (2022). Antibiotic resistance. https://www.who.int/news-room/fact-sheets/detail/antibiotic-resistance

[16] Xiong, G., Wu, Z., Yi, J., Fu, L., Yang, Z., Hsieh, C., Yin, M., Zeng, X., Wu, C., Lu, A., Chen, X., Hou, T., & Cao, D. ADMETlab 2.0: An integrated online platform for accurate and comprehensive predictions of ADMET properties. Nucleic Acids Research, 2021; 49(W1), W5-W14. https://doi.org/10.1093/nar/gkab255

[17] Zhou, X. Y., Ye, X. G., He, L. T., Zhang, S. R., Wang, R. L., Zhou, J., & He, Z. S. In vitro characterization and inhibition of the interaction between ciprofloxacin and berberine against multidrug-resistant Klebsiella pneumoniae. The Journal of Antibiotics, 2016; 69(10), 741-746.

[18] Abraham, M. J., Murtola, T., Schulz, R., Páll, S., Smith, J. C., Hess, B., & Lindahl, E. GROMACS: High performance molecular simulations through multi-level parallelism from laptops to supercomputers. SoftwareX, 2015; 1, 19-25.

[19] Jo, S., Kim, T., Iyer, V. G., & Im, W. CHARMM-GUI: A web-based graphical user interface for CHARMM. Journal of Computational Chemistry, 2018; 29(11), 1859-1865.

[20] Humphrey, W., Dalke, A., & Schulten, K. VMD: Visual molecular dynamics. Journal of Molecular Graphics, 1996;14(1), 33-38.

[21] Wang, E., Sun, H., Wang, J., Wang, Z., Liu, H., Zhang, J. Z., & Hou, T. End-point binding free energy calculation with MM/PBSA and MM/GBSA: Strategies and applications in drug design. Chemical Reviews, 2019; 119(16), 9478-9508.

[22] Valdés-Tresanco, M. S., Valdés-Tresanco, M. E., Valiente, P. A., & Moreno, E. gmx_MMPBSA: A new tool to perform end-state free energy calculations with GROMACS. Journal of Chemical Theory and Computation, 2021; 17(10), 6281-6291.

[23] Elbager, S. G., Elsheikh, M. A., Mohamed, M. A., Elamin, M. H., Ahmed, E. M., & Mohamed, A. O. Identification of potential drug targets and prediction of the potential impact of high risk non-synonymous single nucleotide polymorphism in SARS-CoV-2 3C like proteinase (3CLpro): A computational approach. ChemRxiv. 2020 https://doi.org/10.26434/chemrxiv.12235181.v1

[24] Guan, L., Yang, H., Cai, Y., Sun, L., Di, P., Li, W., Liu, G., & Tang, Y. ADMET-score–a comprehensive scoring function for evaluation of chemical drug-likeness. MedChemComm, 2019; 10(1), 148-157.

[25] Amin, M. L. P-glycoprotein inhibition for optimal drug delivery. Drug Target Insights, 2013; 7, 27-34.

[26] Berellini, G., Waters, N. J., & Lombardo, F. In silico prediction of total human plasma clearance. Journal of Chemical Information and Modeling, 2012; 52(8), 2069-2078.

[27] Aier, I., Varadwaj, P. K., & Raj, U. Structural insights into conformational stability of both wild-type and mutant EZH2 receptor. Scientific Reports, 2016; 6(1), 34984.

[28] Ghahremanian, S., Rashidi, M. M., Raeisi, K., & Toghraie, D. Molecular dynamics simulation approach for discovering potential inhibitors against SARS-CoV-2: A structural review. Journal of Molecular Liquids, 2022; 354, 118901.

[29] Parida, P. K., Paul, D., & Chakravorty, D. The natural way forward: Molecular dynamics simulation analysis of phytochemicals from Indian medicinal plants as potential inhibitors of SARS-CoV-2 targets. Phytotherapy Research, 2020; 34(12), 3420-3433.

[30] Cummings, J., Aisen, P. S., DuBois, B., Frölich, L., Jack, C. R., Jones, R. W., Morris, J. C., Raskin, J., Dowsett, S. A., & Scheltens, P. Drug development in Alzheimer's disease: The path to 2025. Alzheimer's Research & Therapy, 2016; 8, 1-12.

[31] Lindahl, E., Hess, B., & Van Der Spoel, D. GROMACS 3.0: A package for molecular simulation and trajectory analysis. Molecular Modeling Annual, 2001; 7, 306-317.

[32] Nwobodo, D. C., Ugwu, M. C., Anie, C. O., Al-Ouqaili, M. T. S., Ikem, J. C., Chigozie, U. V., & Saki, M. Antibiotic resistance: The challenges and some emerging strategies for tackling a global menace. Journal of Clinical Laboratory Analysis, 2022; 36(9), e24655. https://doi.org/10.1002/jcla.24655

[33] World Health Organization. (2021). Antimicrobial resistance. https://www.who.int/news-room/fact-sheets/detail/antimicrobial-resistance

[34] Farhadi, F., Khameneh, B., Iranshahi, M., & Iranshahy, M. Antibacterial activity of flavonoids and their structure-activity relationship: An update review. Phytotherapy Research, 2019; 33(1), 13-40.

[35] Fatemi, N., Sharifmoghadam, M. R., Bahreini, M., Khameneh, B., & Shadifar, H. Antibacterial and synergistic effects of herbal extracts in combination with amikacin and imipenem against multidrug-resistant isolates of Acinetobacter. Current Microbiology, 2020; 77, 1959-1967.

[36] Bazzaz, B. S. F., Khameneh, B., Namazi, N., Iranshahi, M., Davoodi, D., & Golmohammadzadeh, S. Solid lipid nanoparticles carrying Eugenia caryophyllata essential oil: The novel nanoparticulate systems with broad-spectrum antimicrobial activity. Letters in Applied Microbiology, 2018; 66(6), 506-513.

[37] Gemeda, N., Tadele, A., Lemma, H., Girma, B., Addis, G., Tesfaye, B., Abebe, A., Gemechu, W., Yirsaw, K., Teka, F., & Gebre-Mariam, T. Development, characterization, and evaluation of novel broad-spectrum antimicrobial topical formulations from Cymbopogon martini (Roxb.) W. Watson essential oil. Evidence-Based Complementary and Alternative Medicine, 2018; 9812093.

[38] Clement, E., Erharuyi, O., Vincent, I., Joy, A., Christopher, A., Abiodun, F., Benedicta, N., Uyi, O., & Osaretin, A. Significance of bitter leaf (Vernonia amygdalina) in tropical diseases and beyond: A review. Malaria Chemotherapy, Control & Elimination, 2014; 3, 120.

[39] Ugbogu, E. A., Emmanuel, O., Dike, E. D., Agi, G. O., Ugbogu, O. C., Ibe, C., & Iweala, E. J. The phytochemistry, ethnobotanical, and pharmacological potentials of the medicinal plant-Vernonia amygdalina L. (bitter leaf). Clinical Complementary Medicine and Pharmacology, 2021 1, 100006.

[40] Kikiowo, B., Ogunleye, A. J., Inyang, O. K., Adelakun, N. S., Enonbun, K. I., Oluyori, A. P., Ogunwa, T. H., & Ogunjimi, A. T. Flavones scaffold of Chromolaena odorata as a potential xanthine oxidase inhibitor: Induced fit docking and ADME studies. BioImpacts, 2020; 10(4), 227-234.

[41] Rabaan, A. A., Halwani, M. A., Garout, M., Alotaibi, J., AlShehail, B. M., Alotaibi, N., Almuthree, S. A., Alshehri, A. A., Alshahrani, M. A., & Othman, B. Exploration of phytochemical compounds against Marburg virus using QSAR, molecular dynamics, and free energy landscape. Molecular Diversity, 2023; 1-18.

[42] Turner, P. (2018). Grace-5.1. 22/qtGrace v 0.2.4.

[43] Tian, W., Chen, C., Lei, X., Zhao, J., & Liang, J. CASTp 3.0: Computed atlas of surface topography of proteins. Nucleic Acids Research, 2018; 46(W1), W363-W367.

[44] Cummings, J., Aisen, P. S., DuBois, B., Frölich, L., Jack, C. R., Jones, R. W., Morris, J. C., Raskin, J., Dowsett, S. A., & Scheltens, P. Drug development in Alzheimer's disease: The path to 2025. Alzheimer's Research & Therapy, 2016; 8, 1-12.

[45] Lindahl, E., Hess, B., & Van Der Spoel, D. GROMACS 3.0: A package for molecular simulation and trajectory analysis. Molecular Modeling Annual, 2001; 7, 306-317.